HHS Public Access

Author manuscript

J Am Chem Soc. Author manuscript; available in PMC 2018 December 28.

Published in final edited form as:

J Am Chem Soc. 2018 June 20; 140(24): 7449–7452. doi:10.1021/jacs.8b04455.

Activationless Multiple-Site Concerted Proton-Electron Tunneling

Miriam A. Bowring[*,†,‡,§], **Liam R. Bradshaw**[‡], **Giovanny A. Parada**[†], **Timothy P. Pollock**[‡], **Ricardo J. Fernández-Terán**[‖], **Scott S. Kolmar**[†], **Brandon Q. Mercado**[†], **Cody W. Schlenker**[‡], **Daniel R. Gamelin**[‡], and **James M. Mayer**[*,†,‡]

[†]Department of Chemistry, Yale University, New Haven, Connecticut 06520, United States

[‡]Department of Chemistry, University of Washington, Seattle, Washington 98195, United States

[§]Department of Chemistry, Reed College, Portland, Oregon 97202, United States

[‖]Department of Chemistry, Angstrom Laboratory, Uppsala University, Box 523, SE 75120 Uppsala, Sweden

Abstract

The transfer of protons and electrons is key to energy conversion and storage, from photosynthesis to fuel cells. Increased understanding and control of these processes are needed. Anew anthracene–phenol–pyridine molecular triad was designed to undergo fast photo-induced multiple-site concerted proton–electron transfer (MS-CPET), with the phenol moiety transferring an electron to the photoexcited anthracene and a proton to the pyridine. Fluorescence quenching and transient absorption experiments in solutions and glasses show rapid MS-CPET (3.2×10^{10} s^{-1} at 298 K). From 5.5 to 90 K, the reaction rate and kinetic isotope effect (KIE) are independent of temperature, with *zero* Arrhenius activation energy. From 145 to 350 K, there are only slight changes with temperature. This MS-CPET reaction thus occurs by tunneling of both the proton and electron, in different directions. Since the reaction proceeds without significant thermal activation energy, the rate constant indicates the magnitude of the electron/proton double tunneling probability.

The coupled movement of electrons and protons drives biological processes such as photosynthesis and cellular respiration. Understanding and mimicking this proton–electron transfer reactivity is valuable for the development of new energy technologies. In some cases, the electron and proton transfer to or from separated sites in the same chemical step. This type of proton–coupled electron transfer (PCET) is termed multiple-site concerted proton electron transfer (MS-CPET) or orthogonal PCET.[1–6] An exemplar of MS-CPET is

[*]**Corresponding Authors:** mbowring@reed.edu, james.mayer@yale.edu.

Supporting Information

The Supporting Information is available free of charge on the ACS Publications website at DOI: 10.1021/jacs.8b04455.

Experimental details and additional results including synthesis and characterization, X-ray crystallographic details, fluorescence and transient absorbance measurements (PDF)

Crystallographic data for **1H** (CIF)

Notes

The authors declare no competing financial interest.

the oxidation of Tyr_Z in photosystem II, with electron transfer (ET) to the oxidized chlorophyll and proton transfer (PT) to the hydrogen bonded histidine.[5] Experimental studies of MS-CPET in hydrogen-bonded phenol-base systems have shown that MS-CPET rates vary with the driving force, Marcus-type intrinsic barriers, and electron and proton donor–acceptor distances.[3,4,7–25]

Theoretical descriptions of PCET reactions usually involve both electron and proton tunneling. This can be described by an overlap of vibronic wave functions, or (in the Born–Oppenheimer limit) as the product of an electronic coupling term and a sum of vibrational wave function overlap integrals.[26,27] Some MS-CPET reactions exhibit experimental hallmarks of proton tunneling, such as significant rates at cryogenic temperatures.[28–32] For instance, MS-CPET was implicated in the photo-oxidation of a phenol–benzimidazole unit at 13 K.[19] Reported here is a study of MS-CPET using a unimolecular anthracene–phenol–pyridine system that undergoes rapid photoinduced MS-CPET via electron and proton tunneling, with little or no thermal activation energy. The system mimics MS-CPET reactivity in biology and provides new insights into this class of reactions.

The anthracene–phenol–pyridine triad **1H** (Figure 1) was designed to undergo favorable and rapid photoinduced MS-CPET. The photoexcited anthracene is a strong oxidant,[7] and the conjugated phenol–pyridine has a low intrinsic barrier to MS-CPET.[11,12] Our prior studies of phenol–base MS-CPET oxidations involved bimolecular reactions; their rates therefore could not exceed the diffusion limit.[7] The unimolecular system **1H** removes this limitation. A methylene spacer was included between the anthracene and phenol–pyridine to keep them electronically distinct at a short distance. The spacer prevents π–π stacking of the phenol–pyridine and anthracene, as shown by the X-ray crystal structure of solid **1H** (Figure 1A). The phenol-pyridine unit has the typical planar structure with a short OH···N hydrogen bond [d(O···N) = 2.566(5) Å].[12,14]

Solutions of compound **1H**, along with O-deuterated and O-methylated analogs **1D** and **1Me**, were studied by time-resolved fluorescence using a photon-counting streak camera (Figure 1B). Irradiation with 362 nm laser pulses selectively excited the anthracene portion of the triads (Figure S12). The emission spectra of **1H**, **1D**, and **1Me** in MeCN at room temperature are similar to the spectrum of free anthracene (Figure S12). The control compound **1Me**, which cannot undergo MS-CPET, has an emission lifetime (5 ns) similar to that of free anthracene.[33] In contrast, **1H** exhibited fast quenching of the anthracene emission. The decay of the emission in MeCN was dominated by a fast component (τ = 31 ps) and showed a minor slow component (≤2%, τ = 8 ns). Fast quenching was also observed in less polar media: fluorescence lifetimes were 56 and 86 ps in 2-methyl-THF (2-MeTHF) or methylcyclohexane (MeCy) solutions, respectively, and 92 ps in poly(methylmethacrylate) (PMMA) films. Triad **1D** showed a fast quenching component in MeCN (τ = 116 ps) that is longer than that of **1H**, corresponding to a primary kinetic isotope effect (KIE) of 3.7 ± 0.4.

UV–vis transient absorption (TA) spectroscopy corroborated the lifetimes measured by fluorescence quenching and indicated an electronically isolated anthracene moiety (Figures 2A, S20–23). For **1H** and **1Me**, the TA data after 365 nm excitation showed spectral features

and decay time constants (4 ps) characteristic of formation and vibrational energy redistribution of the S_1 anthracene excited state (S_1-anth*).[34,35] Thus, both the fluorescence and TA show that the CH_2–phenol–pyridine substituent does not affect the S_1-anth*.

The S_1-anth* in **1Me** persists for more than 1 ns, while the corresponding state in **1H** decays with $\tau = 28$ ps. These values are in agreement with the 5 ns and 31 ps decays measured by fluorescence quenching. The decay of the **1H** excited state is slower than vibrational cooling, so quenching occurs predominantly from the thermally equilibrated anthracene local excited state.

The rate constants and isotope effects implicate an MS-CPET mechanism for the quenching in **1H** and **1D**. This mechanism involves ET from the phenol–pyridine to the S_1-anth* local excited state in concert with PT across the OH···py hydrogen bond (Scheme 1). The quenching rate constant for **1H**, $k = 3.2 \times 10^{10}$ s^{-1} in MeCN must correspond to a unimolecular process because it is faster than diffusional collisions between dilute solutes. The primary KIE of 3.7 between **1H** and **1D** implies that the hydrogen/deuterium nucleus is involved in the process. Förster and Dexter energy transfer are unlikely quenching mechanisms. The anthracene emission and the phenol–pyridine absorption show negligible spectral overlap (Figure S12) and indicate that energy transfer would be energetically uphill (FMO analysis, Supporting Information). The driving force for MS-CPET can be roughly estimated as −9 kcal mol^{-1}, the value for the related bimolecular reaction.[7] The unlikelihood of Förster and Dexter energy transfer is further supported by the unperturbed nature of the initially formed S_1-anth* state and by **1Me** exhibiting nearly identical photophysical behavior to free anthracene. Additionally, phenol–imine excited states often exhibit emission in the visible range,[36] but photoexcited samples of **1H** showed emission only from anthracene, suggesting that phenol–imine excited states were not present and energy transfer did not occur. The data presented here, together with published results on bimolecular oxidations of similar phenol–base compounds (including with excited anthracene),[3,4,7–25] all indicate the MS-CPET mechanism in Scheme 1.

The photoinduced fluorescence of **1H** was measured over a large temperature range (Figure 3A). The fast decay rates are insensitive to temperature: they vary *only by a factor of 2 over the temperature range 5.5–350 K* in 2-MeTHF. Emission from **1Me** has a nearly constant long lifetime over the entire temperature range. The quenching rate for **1H** at 5.5 K is unaffected by the incident laser power over a range from 0.1 to 1.4 mW, so local heating and multiphoton effects are not significant. The long-lived minor slow component of the fluorescence decay becomes more pronounced at lower temperatures, to a degree that depends on the medium (up to ~40% in 2-MeTHF, up to ~20% in PMMA at 5.5 K). This long-lived component could correspond to a different conformer of **1H** and could relate to the weak long-lived signal seen in the TA spectra (Figure 2B), which we have been unable to assign with confidence. The MS-CPET zwitterionic photoproduct (Scheme 1) is expected to be difficult to observe because it would likely rapidly convert back to the **1H** ground state, due to a driving force for decay that can be roughly estimated as −64 kcal mol^{-1}. This driving force corresponds approximately to the 0–0 transition energy (~390 nm/73 kcal mol^{-1}) less the MS-CPET driving force (~ −9 kcal mol^{-1}).

The Arrhenius plot of MS-CPET rate constants for **1H** in 2-MeTHF (Figure 3B) has unusual features. First, the range of temperatures is large, from 5.5 to 350 K, *a factor of 64 in temperature*. Second, the range of rate constants is extremely small: the $k_{MS\text{-}CPET}$ for **1H** are all within *less than one In unit*. Within this scale, the Arrhenius plot has two distinct regimes. In the low-temperature regime (5.5 to 85 K), $k_{MS\text{-}CPET}$ is *constant* at $[1.2 \pm 0.1] \times 10^{10}$ s^{-1}. The best fit to the Arrhenius equation gives *zero* activation energy ($E_a = 0.0 \pm 0.01$ kcal mol^{-1}) and a small pre-exponential factor ($A = [1.2 \pm 0.1] \times 10^{10}$ s^{-1}). At higher temperatures, 145 to 350 K, $k_{MS\text{-}PET}$ increases only slightly, by a factor of 2. The Arrhenius plot in this regime is slightly curved, and the approximate parameters extracted from it are unusually small: $A = 2.9 \times 10^{10}$ s^{-1} and $E_a = 0.33$ kcal mol^{-1}.

The MS-CPET rate constants were measured for **1H** in PMMA, which is a glass at all temperatures studied. The same distinct temperature regimes were observed as in 2-MeTHF, but without the discontinuity (Figure 3C). Thus, the change in E_a with temperature is a property of **1H** and is not caused by the glass transition in 2-MeTHF, while the small discontinuity observed in 2-MeTHF may be an effect of the glass transition.

The fluorescence lifetimes for the major fast component varied slightly in different glasses at 5.5 K, with values of 88 ps (MeCy), 94 ps (2-MeTHF), and 151 ps (PMMA). The slower component became more pronounced at low temperatures, perhaps reflecting a temperature- and solvent-dependent distribution of conformers of **1H** that do not interconvert on the time scale of the MS-CPET reaction. The mechanistic conclusions below are for the predominant fast component.

The temperature dependence of $k_{MS\text{-}CPET}$ for **1D** in 2-MeTHF is similar to that for **1H** (Figure 3B). It has an Arrhenius slope of zero in the low-temperature regime, and a small $E_a(D) = 0.48$ kcal mol^{-1} between 145 and 350 K. The KIE is constant at 2.7 ± 0.3 from 5.5 to 85 K and varies from ± 0.5 at 175 K to 1.8 ± 0.2 at 350 K ($E_a(D) - E_a(H) = 0.2$ kcal mol^{-1}). The room-temperature KIE values support an MS-CPET mechanism because they are similar to values measured for thermal *bimolecular* MS-CPET reactions of related phenol–pyridines (~2.7 in MeCN).[12]

Overall, MS-CPET in **1H** has unusual kinetic features. The reactions are fast even at 5.5 K, with zero Arrhenius activation energy up to 80 K, and small sensitivity to the surrounding medium. The temperature independence of the KIE at low temperatures is a marker for proton tunneling.[37] Together, these results indicate that the electron and proton both transfer by tunneling from a thermodynamic minimum configuration, with essentially no nuclear reorganization. At higher temperatures, MS-CPET in **1H** has a very small Arrhenius activation energy of 0.33 kcal mol^{-1} (115 cm^{-1}) in 2-MeTHF. Given this small value and the insensitivity of $k_{MS\text{-}CPET}$ to the medium, this energy may reflect thermal excitation of a vibration modulating the proton donor–acceptor (O···N) distance.[26] In a simple tunneling model, the fast rates and small KIE's observed would correspond to a short O···N distance and a narrow barrier. A much more complete theoretical treatment of the system is needed to include, for instance, the role of vibrational excited states.[13,26]

Since MS-CPET in **1H** below 85 K proceeds without thermal activation, its rate constant is limited only by the probability of the proton/electron double tunneling event. The theoretical maximum rate constant for electron or proton transfer is on the order of 10^{13} s^{-1}, based on the maximum rate of activationless electron transfer and the period of skeletal vibrations.[10,38,39] Thus, the $k_{MS\text{-}CPET}$ for **1H** of ~10^{10} s^{-1} implies that the probability of the concerted electron/proton tunneling process is about 10^{-3}. The probability corresponds to a prefactor for an exponential, like κ in transition state theory, and is consistent with a nonadiabatic process. It represents a rare direct experimental determination of a reaction probability for a proton-coupled electron transfer process.

In conclusion, photoexcited **1H** undergoes fast intramolecular electron and proton transfer in different directions in a single kinetic step, even at 5.5 K. The temperature insensitivity of the reaction rate indicates an important limiting case in which the charge separation reaction is not thermally activated and proceeds via simultaneous tunneling of the electron and proton. The measured rates allow direct experimental determination of the approximate probability of proton–electron tunneling (~10^{-3}). The simple molecular system examined here shows how to achieve rapid and barrierless MS-CPET, which could be relevant to biological processes and new energy technologies.

Supplementary Material

Refer to Web version on PubMed Central for supplementary material.

ACKNOWLEDGMENTS

The authors thank Adam E. Colbert, David S. Ginger (thin film preparation); Belinda Pettersson, Leif Hammarström (TA at Uppsala University); TuKiet Lam (obtaining and analyzing high resolution mass spectra, Yale University); Ethan L. Fisher, Brian Skinner, Todd F. Markle, Miles W. Johnson, and Maraia E. Ener (helpful discussions). This work was and supported by NIH Grants 5R01GM050422 and 5F32GM109637.

REFERENCES

(1). Weinberg DR; Gagliardi CJ; Hull JF; Murphy CF; Kent CA; Westlake BC; Paul A; Ess DH; McCafferty DG; Meyer TJ Chem. Rev 2012, 112, 4016–4093. [PubMed: 22702235]

(2). Hammes-Schiffer S Chem. Rev 2010, 110, 6937–7100. [PubMed: 21141827]

(3). Biczok L; Linschitz HJ Phys. Chem 1995, 99, 1843–1845.

(4). Nomrowski J; Wenger OS Inorg. Chem 2015, 54, 3680–3687. [PubMed: 25781364]

(5). Barry BA; Chen J; Keough J; Jenson D; Offenbacher A; Pagba CJ Phys. Chem. Lett 2012, 3, 543–554.

(6). Stubbe J; Nocera DG; Yee CS; Chang MC Y. Chem. Rev. 2003, 103, 2167–2202.

(7). Schrauben JN; Cattaneo M; Day TC; Tenderholt AL; Mayer JM J. Am. Chem. Soc 2012, 134, 16635–16645. [PubMed: 22974135]

(8). Markle TF; Tronic TA; DiPasquale AG; Kaminsky W; Mayer JM J. Phys. Chem. A 2012, 116, 12249–12259. [PubMed: 23176252]

(9). Markle TF; Rhile IJ; Mayer JM J. Am. Chem. Soc 2011, 133, 17341–17352. [PubMed: 21919508]

(10). Markle TF; Rhile IJ; DiPasquale AG; Mayer JM Proc. Natl. Acad. Sci. U. S. A 2008, 105, 8185–8190. [PubMed: 18212121]

(11). Markle TF; Mayer JM Angew. Chem., Int. Ed 2008, 47, 738–740.

(12). Rhile IJ; Markle TF; Nagao H; DiPasquale AG; Lam OP; Lockwood MA; Rotter K; Mayer JM J. Am. Chem. Soc 2006, 128, 6075–6088. [PubMed: 16669677]

(13). Glover SD; Parada GA; Markle TF; Ott S; Hammarström LJ Am. Chem. Soc 2017, 139, 2090–2101.

(14). Markle TF; Zhang M-T; Santoni M-P; Johannissen LO; Hammarström LJ Phys. Chem. B 2016, 120, 9308–9321.

(15). Chen J; Kuss-Petermann M; Wenger OS J. Phys. Chem. B 2015 119, 2263–2273. [PubMed: 25078952]

(16). Kuss-Petermann M; Wolf H; Stalke D; Wenger OS J. Am. Chem. Soc 2012, 134, 12844–12854. [PubMed: 22809316]

(17). Mora SJ; Odella E; Moore GF; Gust D; Moore TA; Moore AL Acc. Chem. Res 2018, 51, 445–453. [PubMed: 29309118]

(18). Ravensbergen J; Antoniuk-Pablant A; Sherman BD; Kodis G; Megiatto JD; Méndez-Hernández DD; Frese RN; van Grondelle R; Moore TA; Moore AL; Gust D; Kennis JT M. J. Phys. Chem. B 2015, 119, 12156–12163.

(19). Megiatto JD, Jr.; Méndez-Hernández DD; Tejeda-Ferrari ME; Teillout A-L; Llansola-Portolés MJ; Kodis G; Poluektov OG; Rajh T; Mujica V; Groy TL; Gust D; Moore TA; Moore AL Nat. Chem 2014, 6, 423–428. [PubMed: 24755594]

(20). Megiatto JD; Antoniuk-Pablant A; Sherman BD; Kodis G; Gervaldo M; Moore TA; Moore AL; Gust D Proc. Natl. Acad. Sci. U. S. A 2012, 109, 15578–15583. [PubMed: 22566659]

(21). Stewart DJ; Brennaman MK; Bettis SE; Wang L; Binstead RA; Papanikolas JM; Meyer TJ J. Phys. Chem. Lett 2011, 2, 1844–1848.

(22). Lachaud F; Quaranta A; Pellegrin Y; Dorlet P; Charlot M-F; Un S; Leibl W; Aukauloo A Angew. Chem., Int. Ed 2005, 44, 1536–1540.

(23). Manbeck GF; Fujita E; Concepcion JJ J. Am. Chem. Soc 2016138, 11536–11549.

(24). Biczók L; Bérces T; Linschitz HJ Am. Chem. Soc 1997, 119, 11071–11077.

(25). Gagliardi CJ; Wang L; Dongare P; Brennaman MK; Papanikolas JM; Meyer TJ; Thompson DW Proc. Natl. Acad. Sci. U. S. A 2016, 113, 11106–11109. [PubMed: 27660239]

(26). Hammes-Schiffer SJ Am. Chem. Soc 2015, 137, 8860–8871.

(27). Tishchenko O; Truhlar DG; Ceulemans A; Nguyen MT J. Am. Chem. Soc 2008, 130, 7000–7010. [PubMed: 18465862]

(28). Boussac A; Sugiura M; Lai TL; Rutherford AW Philos. Trans. R. Soc., B 2008, 363, 1203–1210.

(29). Faller P; Rutherford AW; Debus RJ Biochemistry 2002, 41, 12914–12920. [PubMed: 12390016]

(30). Ley D; Gerbig D; Schreiner PR Org. Biomol. Chem 2012, 10, 3781–3790. [PubMed: 22402570]

(31). Meisner J; Kastner J Angew. Chem., Int. Ed 2016, 55, 54005413.

(32). O'Ferrall RA M. J. Phys. Org. Chem. 2010, 23, 559–560.

(33). Nijegorodov N; Vasilenko V; Monowe P; Masale M Spectrochim. Acta, Part A 2009, 74, 188–194.

(34). Emmerling F; Lettenberger MJ Phys. Chem 1996, 100, 19251–19256.

(35). Sepiol JJ Lumin. 1986, 36, 115–120.

(36). LeGourriérec D; Kharlanov V; Brown RG; Rettig WJ Photochem. Photobiol., A 1998, 117, 209–216.

(37). Nagel ZD; Klinman JP Nat. Chem. Biol 2009, 5, 543–550. [PubMed: 19620995]

(38). Winkler JR; Gray HB Chem. Rev 1992, 92, 369–379.

(39). Newton M; Sutin N Annu. Rev. Phys. Chem 1984, 35, 437–480.

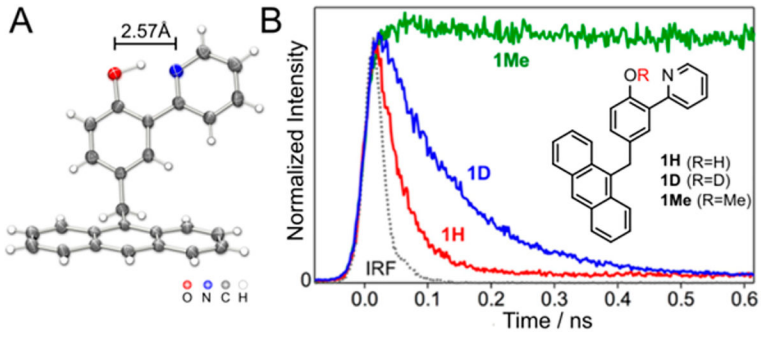

Figure 1.

(A) X-ray crystal structure of **1H**. (B) Time evolution of fluorescence from **1H** (red), **1D** (blue), and **1Me** (green) in acetonitrile at 298 K after excitation at 362 nm. Dotted line = instrument response function.

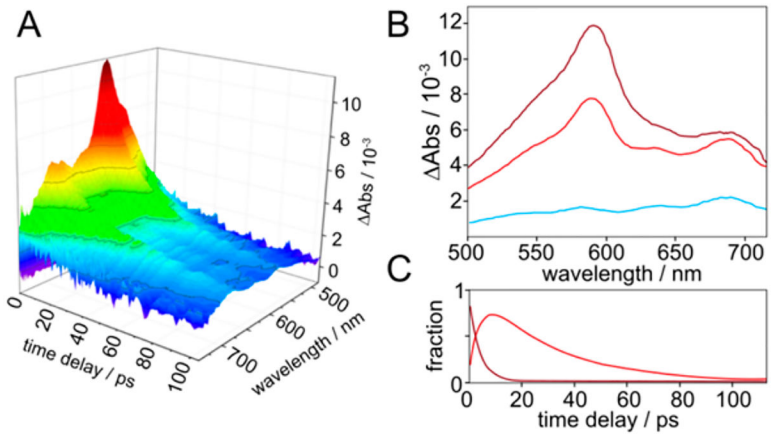

Figure 2.

(A) TA spectra of **1H** in MeCN up to 100 ps after photoexcitation. (B) Component transient absorption spectra from global analysis of spectra from 0 to 100 ps: initial excited state (maroon), vibrationally cooled S_1-anth* state (red), and long-lived photoproduct (cyan). (C) Mole fractions of initial and cooled anth* states.

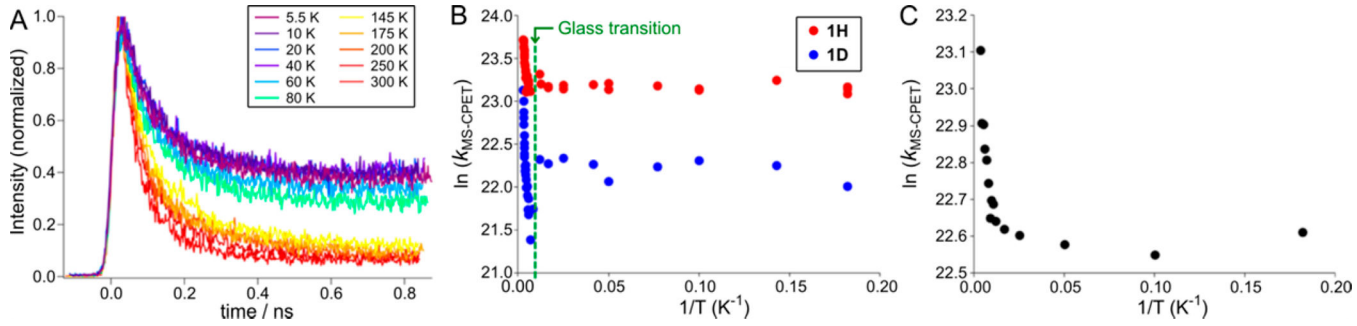

Figure 3.

(A) Time dependence of the fluorescence decay of **1H** in 2-MeTHF from 5.5 to 300 K. (B) Arrhenius plots for **1H** (red) and **1D** (blue) in 2-MeTHF. (C) Arrhenius plot for **1H** in a PMMA film. For (B) and (C), the experimental uncertainties in $\ln(k_{\text{MS-CPET}})$ and $1/T$ are smaller than the size of the data points.

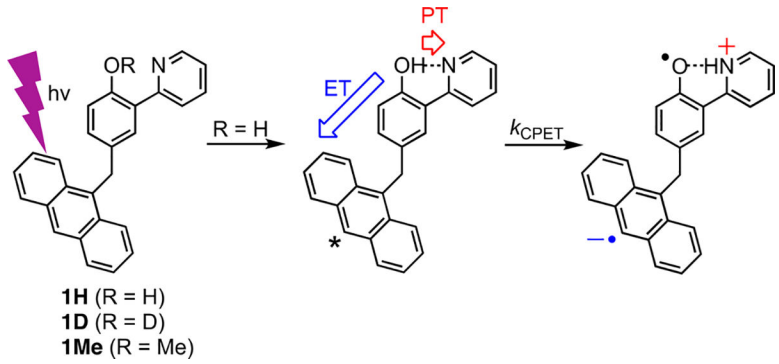

Scheme 1.
MS-CPET Mechanism for Excited State Quenching in 1H